Journal of Membrane Science 736 (2025) 124627

Contents lists available at ScienceDirect

Journal of Membrane Science

journal homepage: www.elsevier.com/locate/memsci

π-Conjugated dibenzothiophene -containing poly(arylene ethylimidazole) copolymers for HT-PEMFCs

Jianan Su [a], Qi Liao [a], Lei Li [a], Lili Sui [b], Jingshuai Yang [a,*], Jin Wang [b,**]

[a] Department of Chemistry, College of Sciences, Northeastern University, Shenyang, 110819, China
[b] School of Pharmacy, Shenyang Medical College, Shenyang, 110034, China

ARTICLE INFO

Keywords:
Imidazole based polymer
π-conjugated dibenzothiophene
High temperature polymer electrolyte membrane
Fuel cell

ABSTRACT

The formation of continuous hydrogen-bond networks in phosphoric acid (PA)-doped high temperature proton exchange membranes (HT-PEMs) is critical for achieving efficient proton transport and high electrochemical performance in HT-PEM fuel cells (HT-PEMFCs). However, conventional PA doped membranes often suffer from a trade-off between mechanical robustness and proton conductivity. In this study, a series of poly(terphenyl-*co*-dibenzothiophene ethylimidazole) (P(TP_x-DBT_{1-x}-EIm)) membranes are synthesized via a one-step superacid-catalyzed polycondensation strategy to overcome this limitation. The incorporation of π-conjugated dibenzothiophene (DBT) introduces a twisted polymer backbone that restricts chain packing and enhances free volume, while the sulfur atoms offer additional hydrogen-bonding sites to facilitate the formation of efficient proton conduction channels. By tuning the terphenyl/DBT molar ratio, the copolymer structure is optimized to achieve a favorable balance between conductivity and mechanical strength. The P($TP_{0.9}$-$DBT_{0.1}$-EIm) membrane exhibited a high acid doping content of 215 %, a proton conductivity of 0.109 S cm^{-1} at 180 °C, and a tensile strength of 13.3 MPa. When implemented in a single H_2/O_2 fuel cell under anhydrous, backpressure-free conditions at 160 °C, the membrane delivered a peak power density of 869 mW cm^{-2}. These results underscore the effectiveness of π-conjugated, sulfur-containing architectures in enhancing proton transport while maintaining mechanical durability, offering a promising pathway toward HT-PEMs for high-efficiency fuel cell applications.

1. Introduction

As environmental pollution and the depletion of fossil energy resources continue to intensify, the development of green, renewable energy sources and advanced energy conversion technologies has become increasingly urgent [1,2]. Among various alternatives, fuel cells stand out due to their high energy conversion efficiency, wide operating temperature range, and scalability, positioning them as a promising solution for future sustainable energy systems [3,4]. High-temperature proton exchange membrane fuel cells (HT-PEMFCs), which operate above 100 °C, offer significant advantages such as accelerated electrode reaction kinetics, enhanced tolerance to CO poisoning, and simplified water and thermal management [4,5]. At the core of HT-PEMFCs lies the high temperature proton exchange membrane (HT-PEM), which differs fundamentally from conventional perfluorosulfonic acid (PFSA) based membranes such as Nafion. PFSA membranes rely on hydration-mediated proton transport and thus perform poorly at elevated temperatures under low humidity conditions [6].

To meet the demanding requirements of HT-PEMFCs, most HT-PEMs incorporate basic polymers doped with low-volatility inorganic acids and must simultaneously exhibit high proton conductivity and sufficient mechanical strength [5,7,8]. Among these, phosphoric acid (PA) doped polybenzimidazole (PBI) remains the benchmark material, owing to its excellent thermal, chemical, and mechanical stability [8–10]. Various strategies including grafting, branching, blending and copolymerization have been developed to further enhance its performance [11–14]. For instance, grafting polyurethane side chains onto PBI has been shown to improve both acid retention and mechanical strength [15]. In another approach, blending poly(4,4′-diphenylether-5,5′-bibenzimidazole) (OPBI) with sterically hindered polyimidazolium ionomers stabilized dihydrogen phosphate species and facilitated PA dissociation, thereby improving proton conductivity [16]. Despite these advances, the use of toxic monomers such as 3,3′,4,4′-tetraaminobiphenyl and the complex synthesis procedures required for PBI derivatives limit their broader

* Corresponding author.
** Corresponding author.
E-mail addresses: yjs@mail.neu.edu.cn (J. Yang), wangjin@symc.edu.cn (J. Wang).

https://doi.org/10.1016/j.memsci.2025.124627
Received 10 July 2025; Received in revised form 22 August 2025; Accepted 29 August 2025
Available online 29 August 2025

applicability [8]. Therefore, the development of new HT-PEMs with improved overall performance and simpler synthesis remains a critical research goal.

Recently, arylene-ether based polymers functionalized with quaternary ammonium (QA) or imidazolium groups have emerged as viable alternatives to PBI, offering efficient proton transport via hydrogen-bond networks with PA molecules [17–19]. However, traditional synthesis of these materials often relies on halogenated reagents, involves multistep procedures, and suffers from limited chemical stability due to the presence of benzyl linkages and aryl-ether bonds [20]. Alternatively, the direct incorporation of basic functional groups, such as imidazole [16,21,22], piperidine [23,24], pyridine [25–29] and quinolone [30,31] into the polymer backbone has proven effective in enhancing chemical stability and facilitating proton conduction.

Among these, imidazole-containing HT-PEMs have attracted particular attention due to their strong interaction with PA and ability to form extended hydrogen-bond networks that support Grotthuss-type proton hopping [8,11,32,33]. In our previous work, we synthesized ether-free aromatic polymers containing imidazole units via Friedel-Crafts hydroxyalkylation between terphenyl and five different imidazole-substituted aldehydes/ketones, systematically investigating how the molecular structure of imidazole affected polymerization behavior and membrane properties [34]. In related studies, Li et al. synthesized poly(isatin-*co*-*p*-terphenyl-imidazole) derivatives and introduced imidazolium groups along aliphatic side chains, which significantly improved mechanical strength, oxidation resistance, and thermal stability compared to unmodified analogs [21]. Meanwhile, Zhang et al. employed biphenyl and imidazole-2-formaldehyde to construct a high-density alkaline network membrane, achieving a peak H_2–O_2 fuel cell power density of 850 mW cm^{-2} at 200 °C [22].

Building on our previous work on poly(*p*-terphenylene methylimidazole) [34–36], we report here a new HT-PEM based on a copolymer synthesized using the more cost-effective and highly reactive monomer 1-ethyl-1H-imidazole-2-formaldehyde (EIm), in place of the commonly used 1-methyl-2-imidazolecarboxaldehyde. In addition, a π-conjugated dibenzothiophene (DBT) moiety was introduced alongside *p*-terphenyl (TP) as a co-monomer. The incorporation of DBT serves multiple purposes: it reduces main-chain rotational freedom, extended conjugation plane, increases free volume [37], and meanwhile provides additional hydrogen-bonding sites via the sulfur atom's lone electron pairs. While DBT units have shown promise for enhancing ion transport in anion exchange membranes [37–39], their use in HT-PEMs remains largely unexplored. By systematically varying the ratio of hydrophobic terphenyl and hydrophilic DBT units in the copolymer series P(TP_x-DBT_{1-x}-EIm), we investigated the resulting structure-property relationships, aiming to optimize the balance between proton conductivity and mechanical performance. The feasibility of these PA doped membranes for use in HT-PEMFCs was subsequently demonstrated through membrane characterization and fuel cell testing.

2. Experimental

2.1. Materials

TP, DBT, EIm, dichloromethane (DCM), methanesulfonic acid (MSA), and trifluoromethanesulfonic acid (TFSA) were purchased from Adamas Reagent Ltd. Additional reagents including *N,N*-dimethylacetamide (DMAC), phosphoric acid (85 wt%) and sodium bicarbonate ($NaHCO_3$) were obtained from Sinopharm Chemical Reagent Co. Ltd. All chemicals were used as received without further purification.

2.2. Synthesis of P(TP_x-DBT_{1-x}-EIm) polymers

Homopolymers P(TP-EIm) and P(DBT-EIm) via Friedel-Crafts hydroxyalkylation polycondensation. TP (8.8 mmol) and EIm (9.5 mmol) were dissolved in 7 mL DCM in a two-neck flask under ice-bath stirring for 10 min. Then, 5 mL of MSA was added, followed by 7 mL of TFSA after 5 more minutes. The ice bath was removed, and the reaction proceeded at room temperature for 1 h, resulting in a dark green viscous mixture. This mixture was then precipitated in a saturated $NaHCO_3$ solution to yield a white fibrous polymer, denoted as P(TP-EIm). Under identical conditions, DBT (8.8 mmol) was used in place of TP to synthesize P(DBT-EIm). To prepare copolymers P(TP_x-DBT_{1-x}-EIm), EIm (9.5 mmol) was kept constant while the total molar amount of TP and DBT was fixed at 8.8 mmol, with molar ratios of TP:DBT = 9:1, 8:2, and 7:3. The resulting polymers are denoted as P(TP_x-DBT_{1-x}-EIm), where x = 0.9, 0.8 and 0.7, respectively. The synthetic routes and chemical structures are illustrated in Fig. 1.

2.3. Membrane fabrication and acid doping

Each polymer was dissolved in DMAC to form a homogeneous solution, cast into petri dishes, and dried at 80 °C to obtain transparent, uniform membranes. These membranes were then immersed in either 85 wt% or 75 wt% PA solutions at 30 °C until a constant weight was achieved. After removing residual surface acid, the membranes were dried under vacuum at 80 °C for 6 h. Then the membrane weight and dimensions were recorded again. The acid doping content (ADC%), area swelling (S%), and volume swelling (V%) were calculated using the following equations:

$$ADC\,/\,\% = \frac{M - M_0}{M_0} \times 100\% \tag{1}$$

$$S\,/\,\% = \frac{S - S_0}{S_0} \times 100\% \tag{2}$$

$$V\,/\,\% = \frac{V - V_0}{V_0} \times 100\% \tag{3}$$

where M and M_0 are the membrane masses after and before PA doping, respectively; S and S_0 denote membrane area, and V and V_0 represent membrane volume after and before doping.

2.4. Characterization

The inherent viscosities of the polymers were measured using an Ubbelohde viscometer in DMAC (100 mg dL^{-1}) at 25 °C. Each sample was pre-rinsed into the viscometer, and three consecutive measurements were averaged. Viscosity was calculated using:

$$\eta = \ln\left(\frac{t}{t_0}\right) / c \tag{4}$$

where t_0 and t are the flow times of the solvent and polymer solution, respectively, and c is the solution concentration.

^{1}H NMR spectra were collected using a Bruker AVANCE-600 MHz spectrometer in DMSO-d_6 with tetramethylsilane (TMS) as the internal standard. FTIR spectra were obtained via attenuated total reflectance (ATR) using a Bruker VERTEX70 FTIR spectrometer. Surface morphology was characterized by scanning electron microscopy (SEM, Hitachi SU8010), and elemental composition was analyzed via X-ray photoelectron spectroscopy (XPS, Shimadzu AXIS Supra+). Microphase separation morphology was investigated using tapping-mode atomic force microscopy (AFM, Bruker Dimension Icon) with a silicon N-type cantilever.

Chemical stability was evaluated in a Fenton reagent (3 wt% H_2O_2 with 4 ppm Fe^{2+}) at 68 °C. Membranes were rinsed, dried, and weighed at predetermined intervals. Fresh Fenton reagent was used for each measurement cycle [19,25]. Thermal stability was assessed using thermogravimetric analysis (TGA) on a NETZSCH analyzer under nitrogen from 50 °C to 600 °C at a heating rate of 10 °C min^{-1}.

To test PA retention under humid conditions, acid doped membranes

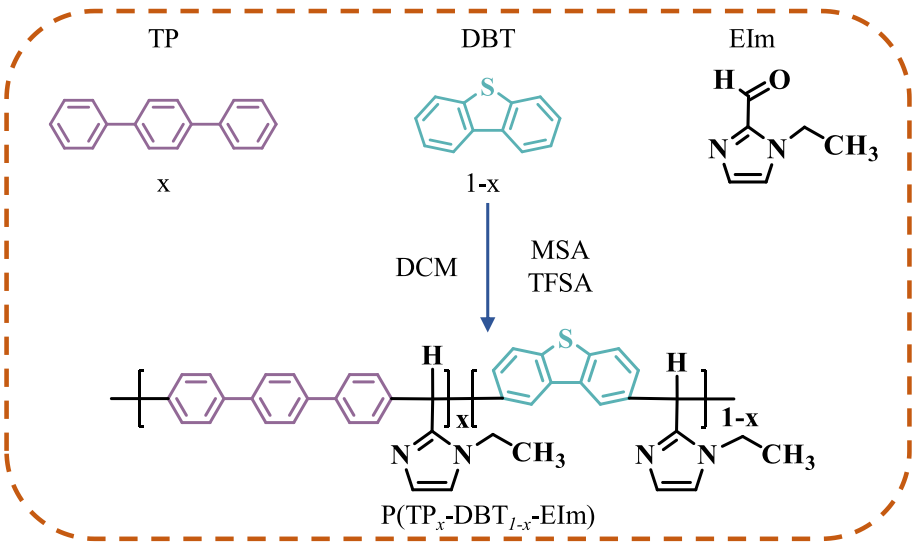

Fig. 1. Synthesis and chemical structures of P(TP$_x$-DBT$_{1-x}$-EIm) copolymers.

were placed in an oven at 80 °C and 40 % relative humidity. Their weight was monitored over time to determine PA loss [9].

The proton conductivity of PA doped membranes was measured via the four-probe method. Samples were dried at 100 °C for 1 h before testing. Resistance (R) was recorded at various temperatures from 100 °C to 180 °C, and conductivity (σ) was calculated as:

$$\sigma = \frac{L}{RS} \tag{5}$$

where L is the distance between electrodes and S is the cross-sectional area of the membrane.

Mechanical properties were measured using a CMT2000 tensile tester (SHIJIN, China) at room temperature. Membrane specimens were cut into dumbbell-shaped strips with a length of 25 mm and width of 4 mm. The test was conducted at a pulling speed of 5 mm min^{-1}. The tensile strength and modulus were calculated from the stress-strain curves.

2.5. Fuel cell performance

Gas diffusion electrodes (GDEs) were fabricated following a previously reported method [40]. Each GDE was prepared with 1.0 mg cm^{-2} loading of Pt/C catalyst using PBI as a binder. A membrane-electrode assembly (MEA) was assembled by hot-pressing two GDEs (active area: 1 cm^2) onto both sides of the acid-doped membrane at 150 °C and 65 kg cm^{-2} for 3 min. The MEA was evaluated under non-humidified H_2/O_2 conditions without backpressure. Flow rates were 120 mL min^{-1} for H_2 and 60 mL min^{-1} for O_2. The polarization curves of the single cell was performed on an electrochemical workstation (BioLogic SP-300).

3. Results and discussions

3.1. Synthesis of polymers and chemical structures

As illustrated in Fig. 1, DBT, EIm, and TP monomers were subjected to a Friedel-Crafts hydroxyalkylation reaction in the presence of TFSA, yielding copolymers containing EIm and DBT segments. Owing to the high reactivity of the three monomers, the polymerization proceeded efficiently within 1 h at room temperature under ambient conditions. The ethylimidazole units promote PA uptake and form proton conducting pathways, while the DBT moieties contribute additional hydrogen-bonding sites and enlarge the free volume. Computational simulations based on P(TP-EIm) and P(DBT-EIm) molecular models were conducted as shown in Fig. 2e and f. The P(TP-EIm) exhibits free volume ratio (22.05 %), while the P(DBT-EIm) had a higher value of 24.78 %, indicating increased accessible 3D surface area and free volume of P(DBT-EIm) comparing to P(TP-EIm). The inherent viscosities of the five synthesized polymers, i.e., P(TP-EIm), P(TP$_{0.9}$-DBT$_{0.1}$-EIm), P(TP$_{0.8}$-DBT$_{0.2}$-EIm), P(TP$_{0.7}$-DBT$_{0.3}$-EIm) and P(DBT-EIm), were 0.97 dL g^{-1}, 1.11 dL g^{-1}, 0.65 dL g^{-1}, 0.56 dL g^{-1} and 3.33 dL g^{-1}, respectively, indicating sufficient molecular weights for membrane fabrication. In addition, the quite high viscosity of P(DBT-EIm) is mainly due to the high reaction activity of DBT monomer as previously reported [37,41].

The chemical structures of P(TP$_x$-DBT$_{1-x}$-EIm) copolymers are confirmed via ^{1}H NMR, FT-IR, and XPS analyses (Fig. 2a–d). In the ^{1}H NMR spectrum of P(DBT-EIm), the signals at 6.97 ppm (H_e) and 7.23 ppm (H_f) correspond to the ethylimidazole ring, while the peaks at 3.91 ppm (H_g) and 1.02 ppm (H_h) arise from the ethyl side chain. The methine proton (–CH–) of the main chain appears at 6.18 ppm (H_d), and the thiophene ring protons resonate from 7.37 ppm to 8.25 ppm ($H_{a\text{-}c}$) [38,42]. For P(TP-EIm), the ethylimidazole peaks appear at 1.15 ppm (H_8), 3.99 ppm (H_7), 6.97 ppm (H_5) and 7.23 ppm (H_6), while the main-chain methine proton is observed at 5.85 ppm (H_4) [34,35]; the aromatic TP protons span from 7.44 ppm to 7.71 ppm ($H_{1\text{-}3}$). The P(TP$_{0.8}$-DBT$_{0.2}$-EIm) copolymer shows its methine proton at 5.81 ppm ($H_{4'}$), imidazole signals at 6.92 ppm and 7.18 ppm ($H_{5',6'}$), and aromatic peaks in the range of 7.34–7.82 ppm ($H_{1'\text{-}3',\ a'\text{-}c'}$). These shifts, slightly lower than in P(DBT-EIm) and slightly higher than in P(TP-EIm), reflect different electron distributions in the TP and DBT aromatic units. Furthermore, as shown in Fig. S1 (Supporting information), integration of the aromatic region in the NMR spectrum indicates that the actual DBT content is approximately 18.8 %, closely matching the targeted 20 %, confirming successful copolymerization.

Infrared spectroscopy (Fig. 2b) further corroborated successful polymer synthesis. The bands at 3022 cm^{-1} are attributed to aromatic C–H stretching, while those at 2920 cm^{-1} and 2850 cm^{-1} correspond to the C–H stretches of the ethyl groups [35]. The imidazole ring's –C–N–C– deformation appears at 1110 cm^{-1}, consistent with reported in literature [43,44]. Slight shifts arise due to the ethyl group's position in EIm and the polymer backbone. The characteristic C–S stretching vibration of the thiophene ring is seen at 1155 cm^{-1}, aligning with previous thiophene IR data [38,39], although slightly shifted due to the benzene rings in DBT. Additionally, XPS spectra of P(TP-EIm), P(TP$_{0.8}$-DBT$_{0.2}$-EIm) and P(DBT-EIm) confirmed sulfur incorporation, as shown in Fig. 2c and d. Two characteristic peaks at ~164 eV correspond

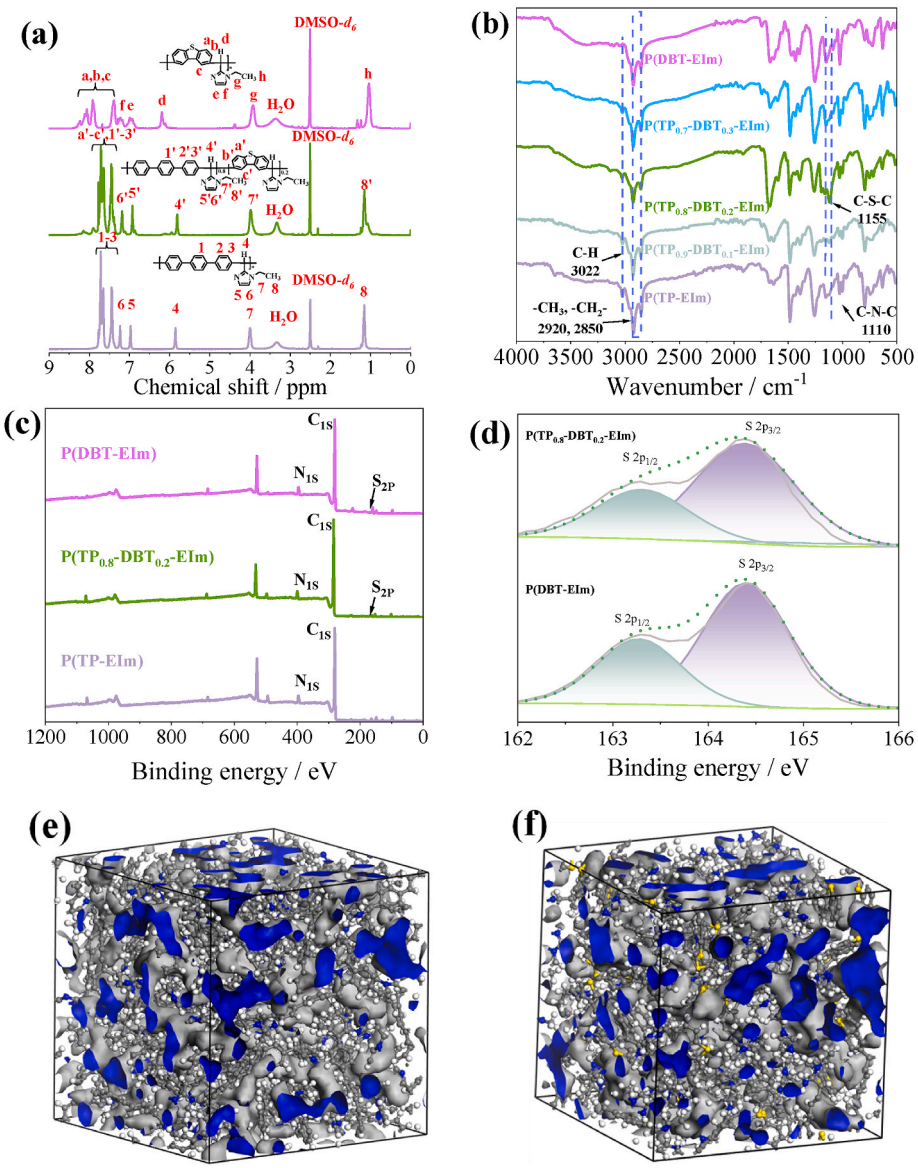

Fig. 2. (a) ^{1}H NMR, (b) FT-IR, (c) XPS and (d) S 2p spectra of various polymers; (e, f) computational simulation structures of P(TP-EIm) and P(DBT-EIm) with accessible areas represented in blue. (For interpretation of the references to color in this figure legend, the reader is referred to the Web version of this article.)

to S 2p$_{1/2}$ and 2p$_{3/2}$ orbitals, consistent with previous reports [45,46]. These results confirm the successful incorporation of DBT into the copolymer backbone.

3.2. Fabrication of membranes and morphology

Five P(TP$_x$-DBT$_{1-x}$-EIm) membranes were fabricated via a simple solution-casting method. As shown in Fig. 3a, all membranes appeared light yellow, smooth, and flexible without cracks or folding. Surface and cross-sectional SEM images (Fig. 3b and c) revealed dense, homogeneous morphologies without visible pores, suggesting good gas barrier properties [7,40]. All membranes exhibited comparable thicknesses, minimizing structural variability during performance comparisons. Furthermore, AFM phase images (Fig. 3d) show that, compared with P(TP-EIm), the P(TP$_x$-DBT$_{1-x}$-EIm) and P(DBT-EIm) membranes exhibit more distinct light and dark contrast, indicating better-developed microphase separation. Fig. S2 shows the binding energies between TP/DBT monomers and water molecules. The binding energy was −3.9 kcal mol^{-1} between the sulfur atom in DBT and water molecule, while the binding energy between TP and water was not available due to the absence of water-binding sites in TP. These findings revealed the hydrophobic nature of TP and the hydrophilic character of DBT. Thus, the incorporation of hydrophilic DBT in copolymer membranes likely promotes phase separation when combined with hydrophobic TP segments. This phase-separated morphology can facilitate the formation of continuous proton-conducting channels, thereby enhancing proton transport [37,39].

3.3. Thermal and chemical stabilities

Thermal stability is a critical parameter for ensuring the long-term durability of HT-PEMs operating under elevated temperatures [4,5]. The thermal degradation profiles and derivative thermogravimetric (DTG) curves of P(TP-EIm), P(TP$_x$-DBT$_{1-x}$-EIm) and P(DBT-EIm) membranes are depicted in Fig. 4a and b. All membranes exhibited negligible weight loss below 190 °C. A slight mass loss (<5 %) was observed between 190 °C and 260 °C in all membranes except P(DBT-EIm), which may be attributed to residual water or unreacted end groups, as the mass loss is much smaller than the proportion of any single component. Notably, P(DBT-EIm), which lacks the terphenyl segment, displayed the

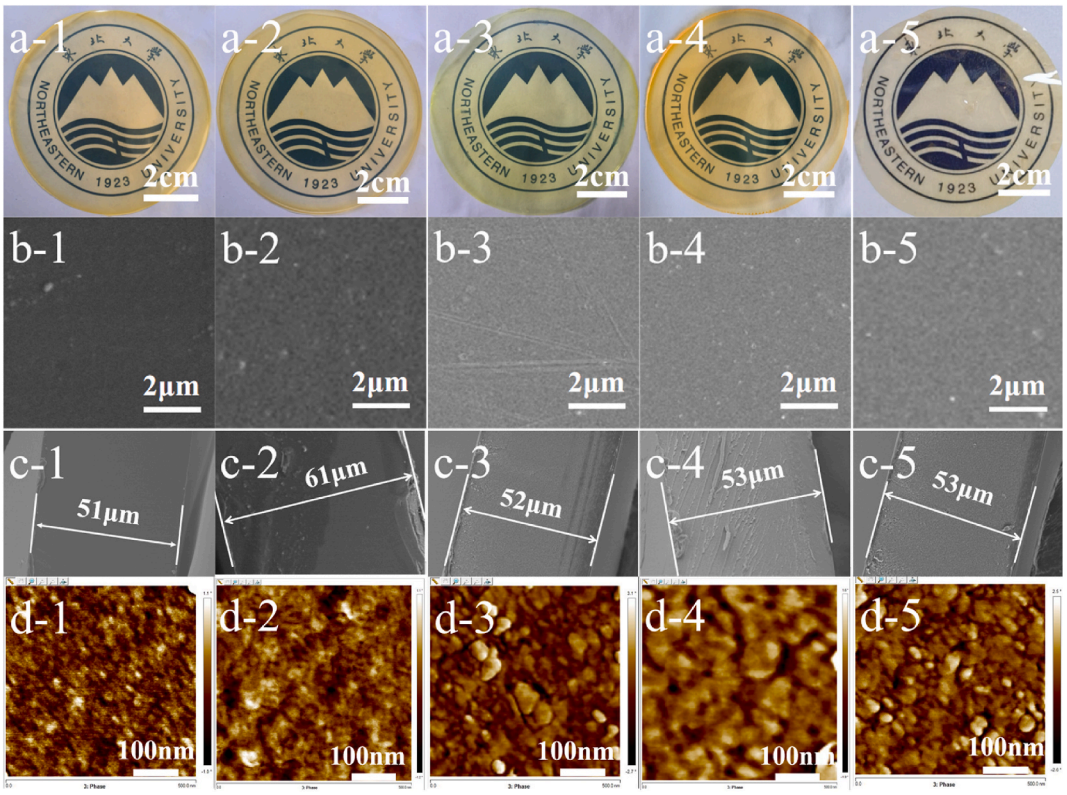

Fig. 3. (a) Photographic, (b) surface SEM, (c) cross-section SEM and (d) AFM images of various membranes including P(TP-EIm) (a-1, b-1, c-1, d-1), P($TP_{0.9}$-$DBT_{0.1}$-EIm) (a-2, b-2, c-2, d-2), P($TP_{0.8}$-$DBT_{0.2}$-EIm) (a-3, b-3, c-3, d-3), P($TP_{0.7}$-$DBT_{0.3}$-EIm) (a-4, b-4, c-4, d-4) and P(DBT-EIm) (a-5, b-5, c-5, d-5).

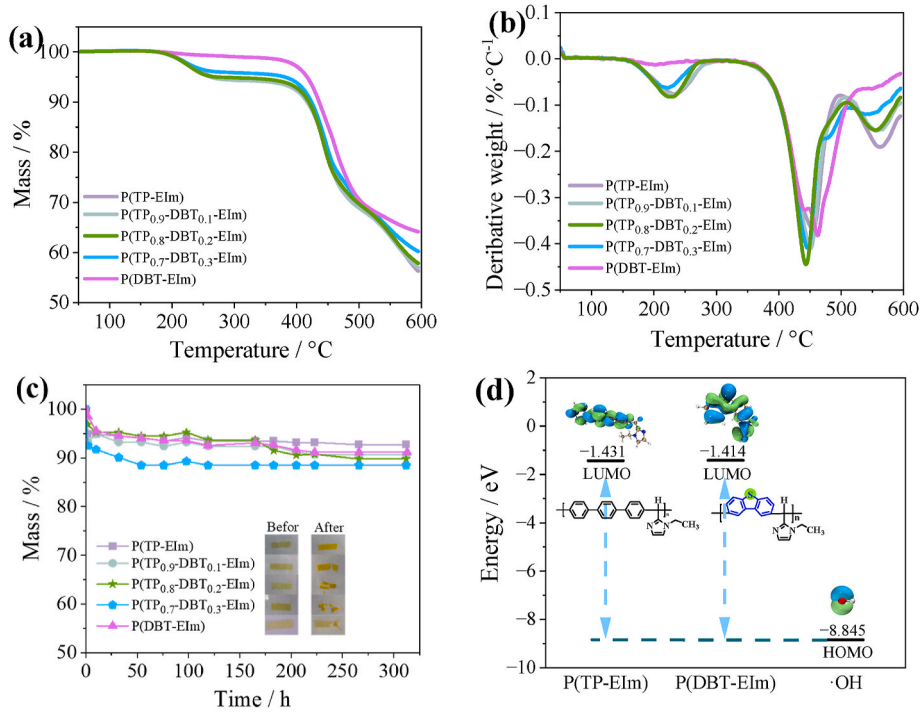

Fig. 4. (a) TGA and (b) DTG curves in N_2, (c) chemical stability via Fenton test (3 wt% H_2O_2 with 4 ppm Fe^{2+} at 68 °C) of various P(TP_x-DBT_{1-x}-EIm) membranes; (d) LUMO and HOMO energy levels of polymer model unit and hydroxyl radical.

onset of decomposition at around 400 °C. The other membranes also began to degrade above 400 °C, likely due to the breakdown of their polymer backbones [34,36]. Overall, the thermal stability of P(TP-EIm) and P(TP_x-DBT_{1-x}-EIm) membranes meets the requirements for HT-PEMFC operation below 180 °C [7,8].

To assess chemical durability, a Fenton test was performed using 3 wt % H_2O_2 solution containing 4 ppm Fe^{2+} at 68 °C, a protocol method for evaluating oxidative stability in HT-PEMs [8,40]. As illustrated in

Fig. 4c, all membranes exhibited a slight initial weight loss, followed by minimal changes from 10 h to 312 h, maintaining over 88 % of their original mass. Notably, the P(TP-EIm) membrane retained more than 92 % of its mass throughout the test duration. However, the P($TP_{0.8}$-$DBT_{0.2}$-EIm) and P($TP_{0.7}$-$DBT_{0.3}$-EIm) membranes fractured after approximately 165 h, which may be attributed to their lower viscosities. This lower molecular weight can lead to increased swelling in the Fenton solution, thereby accelerating oxidative degradation due to enhanced radical penetration. In contrast, the other membranes with higher viscosities retained their structural integrity for the entire 312-h test period, suggesting better resistance to radical-induced damage.

To further elucidate the structure-property relationship governing oxidative resistance, density functional theory (DFT) calculations were conducted on model units representing P(TP-EIm) and P(DBT-EIm). As shown in Fig. 4d, the oxidation process is driven by electron transfer from the highest occupied molecular orbital (HOMO) of the hydroxyl radical (·OH) to the lowest unoccupied molecular orbital (LUMO) of the polymer unit. The energy gap between these orbitals reflects the polymer's resistance to radical attack, a larger gap indicates stronger oxidative stability. The calculated LUMO energy levels for P(DBT-EIm) and P(TP-EIm) were −1.414 eV and −1.431 eV, respectively, while the HOMO of ·OH was −8.845 eV. These similar HOMO-LUMO gaps indicate that both polymer structures exhibit comparable resistance to radical oxidation, which aligns well with the Fenton test results.

3.4. Acid doping, swelling and PA retention

The absorbed PA plays a pivotal role in determining both the proton conductivity and mechanical robustness of HT-PEMs [5,8,31]. As shown in Fig. 5a and b, the ADC% and dimensional swelling behaviors of the membranes were assessed after immersion in 75 wt% and 85 wt% PA solutions at 30 °C. Owing to the pendant and freely rotating ethyl-imidazole (EIm) groups, the P(TP-EIm) membrane exhibited substantial ADC values of 144 % and 198 % in 75 wt% and 85 wt% PA, respectively. These high doping levels can be attributed to strong acid-base interactions and hydrogen bonding between the imidazole units and PA molecules [34,36]. Furthermore, the P(TP_x-DBT_{1-x}-EIm) copolymer membranes showed a progressive increase in ADC with rising dibenzothiophene content. Specifically, the ADC increased markedly from 215 % to 326 % as the DBT molar fraction increased from 10 % to 30 %. This enhancement is likely due to the disruption of polymer chain packing and the introduction of additional free volume caused by the π-conjugated DBT segments [37,38]. Remarkably, the P(DBT-EIm) homopolymer exhibited extremely high ADC values, i.e., 1069 % and 1670 % in 75 wt% and 85 wt% PA, respectively. However, the high PA uptake significantly compromised the mechanical integrity of the membrane, rendering it too soft and fragile for practical handling. To address this, rigid *p*-terphenyl units were incorporated into the copolymer backbone to enhance mechanical stability and suppress excessive swelling. As seen in Fig. 5b, increasing the TP content in the copolymer effectively reduced dimensional swelling, primarily due to decreased PA uptake. For instance, the P($TP_{0.9}$-$DBT_{0.1}$-EIm)/215 %PA membrane exhibited significantly lower area and volume swellings (66 % and 150 %, respectively) compared to the more PA doped counterpart P($TP_{0.7}$-$DBT_{0.3}$-EIm)/326 %PA (103 % and 232 %).

To gain deeper insight into the molecular-level interactions between PA and different polymer backbones, theoretical calculations were performed to evaluate the binding energies between PA molecules and the repeat units. Geometry optimizations were conducted at the B3LYP/6-31G(d) level, with convergence criteria set to energy changes smaller than 1×10^{-6} Hartree. Single-point energy calculations were carried out on the optimized structures using the same functional and basis set. Model structures of P(TP-EIm) and P(DBT-EIm) with hydrogen-terminated repeating units were employed for simulations. All calculations were performed in vacuum without solvent effects or dispersion corrections [41]. These results provide fundamental understanding of how heteroatoms (e.g., nitrogen and sulfur) and polymer chain conformations influence PA affinity. As illustrated in Fig. 5c, the nitrogen atom in the EIm unit of P(TP-EIm) binds to a PA molecule with a calculated binding energy of −17.20 kcal mol^{-1}. In P(DBT-EIm), two distinct

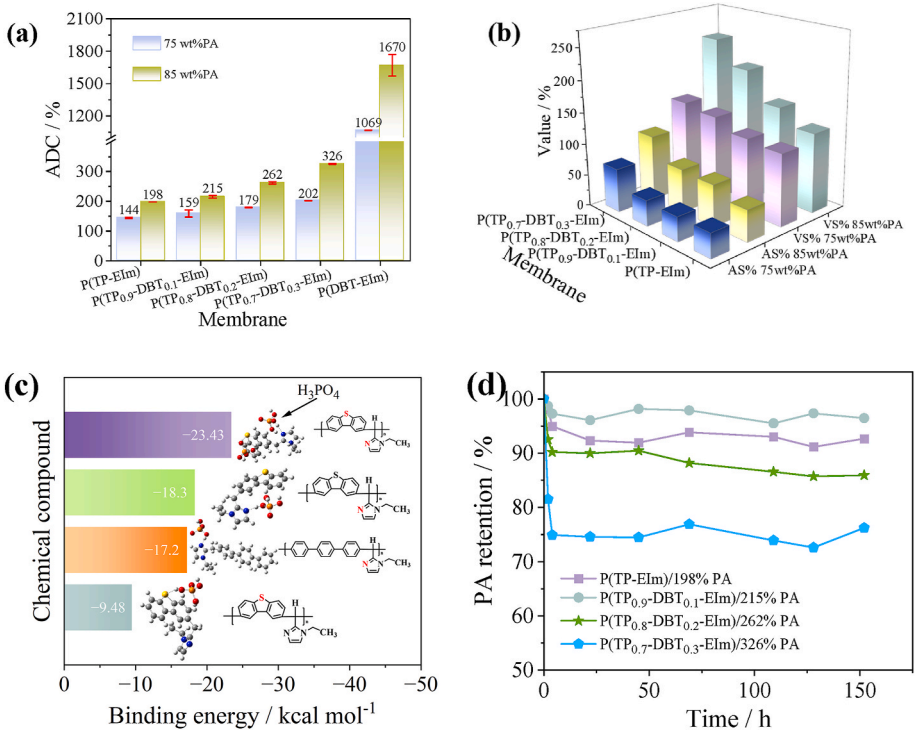

Fig. 5. (a) ADC%, (b) dimensional swellings of various membranes doping in 75 wt% and 85 wt% PA solutions at 30 °C; (c) binding energies between the red-color group in P(DBT-EIm)/P(TP-EIm) repeat unit and PA molecules; (d) PA retention ratio of different PA doped membranes at 80 °C and 40 % RH. (For interpretation of the references to color in this figure legend, the reader is referred to the Web version of this article.)

binding sites exist: the nitrogen in EIm and the sulfur in the DBT unit, with binding energies of −18.30 and −9.48 kcal mol^{-1}, respectively. When two PA molecules simultaneously bind to both the nitrogen and sulfur sites, the total binding energy is −23.43 kcal mol^{-1}, which was lower than the sum of the two isolated interactions (−27.78 kcal mol^{-1}). Nonetheless, the presence of DBT clearly enhances PA affinity by introducing additional hydrogen-bonding sites, which could in turn facilitate improved proton conduction.

Since PA molecules are the primary proton carriers in HT-PEMs, their retention within the membrane matrix is crucial for long-term durability and consistent fuel cell performance [7,47]. The PA retention behavior of the membranes was evaluated over 160 h at 80 °C and 40 % relative humidity (Fig. 5d). Most of the PA loss occurred within the first 4 h, likely due to desorption of loosely bound surface acid. Thereafter, the PA content gradually stabilized. Among the tested samples, the P($TP_{0.9}$-$DBT_{0.1}$-EIm)/215 %PA membrane with DBT segments retained 96.5 % of its initial PA content after 160 h, outperforming the P(TP-EIm)/198 %PA membrane under identical conditions. This improvement is attributed to the enhanced hydrogen-bonding interactions enabled by DBT, which restrict PA mobility and mitigate leaching. However, at higher DBT contents, such as in P($TP_{0.8}$-$DBT_{0.2}$-EIm) and P($TP_{0.7}$-$DBT_{0.3}$-EIm), PA retention decreased, likely due to excessive PA doping contents, where excess free PA molecules might be more prone to evaporation or diffusion [47]. Therefore, optimizing the DBT-to-TP ratio in the copolymers is key to achieving a desirable balance between high PA uptake, dimensional stability and PA retention.

3.5. Proton conductivity and mechanical properties

Proton conductivity is a critical parameter for evaluating the performance of HT-PEMs in fuel cells [8,36]. As shown in Fig. 6a, all membranes exhibited increasing proton conductivity from 100 °C to 180 °C under anhydrous conditions, primarily due to enhanced proton mobility and thermally assisted diffusion at elevated temperatures [5,34]. For instance, the proton conductivity of the P(TP-EIm)/198 %PA membrane rose from 0.042 S cm^{-1} at 100 °C to 0.079 S cm^{-1} at 180 °C. In comparison, the PA-doped P(TP_x-DBT_{1-x}-EIm) membranes demonstrated even higher conductivities, attributable to the presence of dibenzothiophene units, which significantly enhanced PA uptake. In general, higher PA doping levels promote stronger hydrogen-bonding networks. As shown in Fig. S3, the E_a values of various PA doped membranes ranged from 7.14 to 15.67 kJ mol^{-1}, supporting proton conduction via the Grotthuss mechanism [5,7]. Moreover, the sulfur-containing DBT segments further facilitate proton transfer by introducing secondary hydrogen-bonding sites, as schematically illustrated in Fig. 6c. Among all tested membranes, the P($TP_{0.7}$-$DBT_{0.3}$-EIm)/326 %PA membrane exhibited the highest conductivity of 0.159 S cm^{-1} at 180 °C, significantly surpassing that of the P(TP-EIm)/198 %PA membrane. Notably, this value is comparable to or even higher than other HT-PEMs reported in literature. For example, the CPyOPBI–OH–20/331 %PA membrane showed a conductivity of 95 mS cm^{-1} at 180 °C [10]; the AG-100/433 %PA membrane exhibited a conductivity of 82 mS cm^{-1} at 160 °C [12]; and the PBI-p-2.72/344 %PA membrane displayed a conductivity of 90 mS cm^{-1} at 160 °C [33].

In addition to proton conductivity, mechanical strength is equally vital to ensure membrane durability during long-term fuel cell operation [8,40]. As shown in Fig. 6b, membranes with lower acid doping content generally exhibited superior mechanical performance, since phosphoric acid acts as a plasticizer and compromises membrane rigidity at high contents [7,34]. For instance, although the P($TP_{0.7}$-$DBT_{0.3}$-EIm)/326 % PA membrane achieved the highest conductivity, its tensile strength at room temperature was only 1.94 MPa due to severe plasticization. By contrast, the P($TP_{0.9}$-$DBT_{0.1}$-EIm) membranes, with ADC% of 159 % and

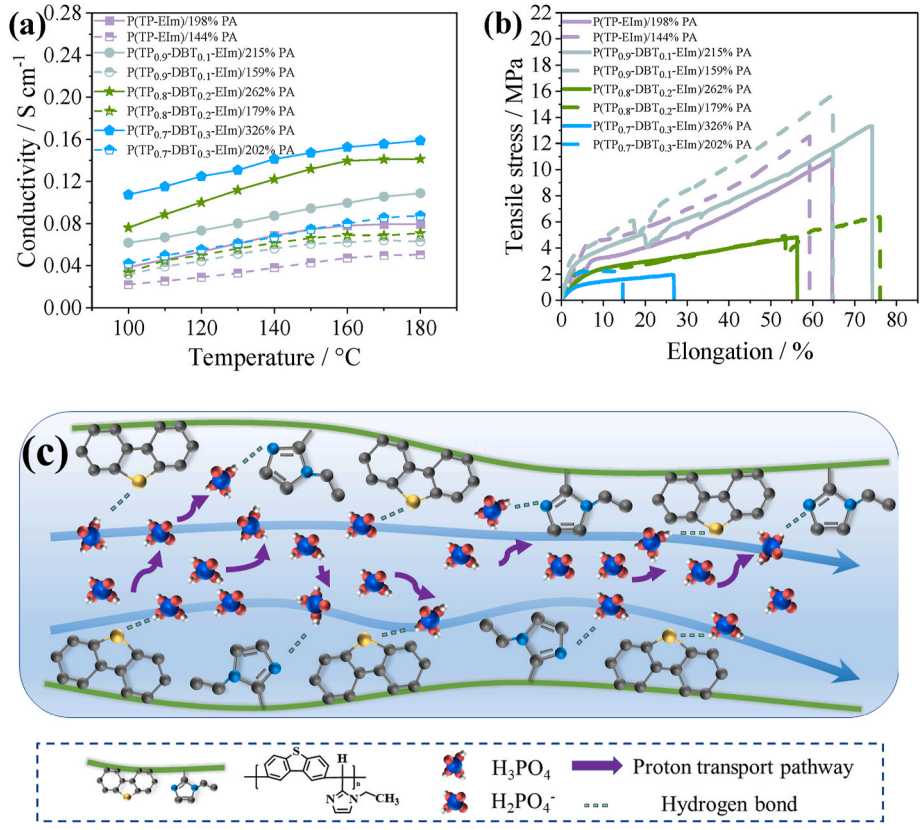

Fig. 6. (a) Proton conductivities as functions of temperature, (b) mechanical stress-strain curves of various PA doped membranes; (c) schematic illustration of possible proton transfer mechanism in the P(DBT-EIm)/PA membrane.

215 %, achieved much higher tensile strengths of 15.6 MPa and 13.3 MPa, respectively. Interestingly, the P($TP_{0.9}$-$DBT_{0.1}$-EIm)/215 %PA membrane exhibited better mechanical strength than other samples with even lower ADC values, such as P($TP_{0.8}$-$DBT_{0.2}$-EIm)/179 %PA, P(TP-EIm)/198 %PA, and P(TP-EIm)/144 %PA. This enhancement likely stems from the higher viscosity and molecular weight of P($TP_{0.9}$-$DBT_{0.1}$-EIm), implying a higher degree of polymerization and stronger interchain interactions, which reinforce structural integrity. Furthermore, the mechanical performance of P($TP_{0.9}$-$DBT_{0.1}$-EIm)/215 %PA rivals or even surpasses that of other HT-PEMs. For instance, the PA-doped BOPBI-PIL-10 % membrane (ADC% = 227 %) exhibited a tensile strength of 6.94 MPa at room temperature [9]; the Q-SCT-NPAEK-80 %/314 %PA membrane reached a tensile strength of 14.1 MPa [17]; while the PTP-10cPIM/149 %PA showed a tensile strength of 13.03 MPa [24].

3.6. Fuel cell performance

Based on a comprehensive evaluation of proton conductivity and mechanical properties, the P($TP_{0.9}$-$DBT_{0.1}$-EIm)/215 %PA membrane with a thickness of 60 μm was selected for single-cell fuel cell performance testing. Polarization curve measurements were performed under non-humidified H_2/O_2 conditions at temperatures ranging from 120 °C to 160 °C. As shown in Fig. 7a, the membrane displayed excellent open circuit voltage (OCV) values between 1.00 V and 0.98 V over the tested temperature range. These values significantly exceed the typical OCVs of conventional HT-PEMFCs (0.90–0.95 V), indicating low gas crossover and minimal hydrogen/oxygen mixing, which helps reduce electrode polarization losses [23]. The peak power density exhibited a strong temperature dependence: 420 mW cm^{-2} at 120 °C, 678 mW cm^{-2} at 140 °C, and reaching 869 mW cm^{-2} at 160 °C. This enhancement is attributed to two primary factors: (1) improved electrode kinetics: higher operating temperatures reducing the activation energy for both the oxygen reduction reaction (ORR) and the hydrogen oxidation reaction (HOR), thereby accelerating charge transfer processes [2,4]; (2) enhanced proton transport: elevated temperatures facilitating the Grotthuss-type hopping mechanism in PA-doped membranes, which significantly boosting proton mobility [5,7]. Furthermore, the superior performance of the P($TP_{0.9}$-$DBT_{0.1}$-EIm)/215 %PA membrane is largely due to the presence of DBT moieties, which promote the formation of extensive hydrogen-bonding networks and enable efficient ion-conducting channels, thereby improving both conductivity and membrane stability. To evaluate acid retention, the P($TP_{0.9}$-$DBT_{0.1}$-EIm)/215 % membrane was tested under fuel cell operating conditions (160 °C, 200 mA cm^{-2}). As presented in Fig. S3, the cell voltage showed nearly constant values over 50 h, suggesting negligible PA loss. Nonetheless, extended durability measurements remain necessary to fully establish the long-term stability of the membrane. Previous studies have estimated an average acid loss rate of 2–4 mg H_3PO_4 cm^{-2} 10000 h of continuous operation for PA-doped PBI membranes [7]. Evaporation is considered the dominant acid loss pathway, strongly affected by parameters such as vapor pressure, reactant gas flow, and cell temperature [47].

To further highlight the advantages of the developed membrane, Fig. 7b compares the peak power densities of various reported HT-PEMs under H_2/O_2 conditions at 160 °C. For instance, a PA-doped polyurethane-grafted PBI reached 405 mW cm^{-2} [15]. Other notable examples include, a three-dimensional polyaniline-crosslinked OPBI membrane: 474 mW cm^{-2} [48]; a semi-flexible PBI membrane (PBI-QP-20): 507 mW cm^{-2} [49]; OPBI/polyimidazolium dihydrogen phosphate composite: 568 mW cm^{-2} [16]; benzimidazole functionalized branched poly(terphenyl trifluoroacetophenone piperidine) with dual proton conductors: 621 mW cm^{-2} [50]; PTP membrane incorporating twisted cPIM for low-PA doping: 694 mW cm^{-2} [24]; hydroxylated/crosslinked OPBI membrane: 710 mW cm^{-2} [10]; Ionic liquid-incorporated PBI membrane: 717 mW cm^{-2} [33]. In comparison, the newly developed P($TP_{0.9}$-$DBT_{0.1}$-EIm)/215 %PA membrane demonstrated a remarkable peak power density of 869 mW cm^{-2}, underscoring its superior performance. In addition, as previously reported by Chen et al., the HT-PEMFC performance depends on multiple operational and structural parameters, including MEA fabrication techniques, gas purity, catalyst types, and the optimization of the three-phase interface [51–53]. Despite these complex influencing factors, the results presented here confirm the great promise of the hydrogen-bond-network-rich P($TP_{0.9}$-$DBT_{0.1}$-EIm)/PA membrane as a next-generation candidate for high-performance HT-PEMFC applications.

4. Conclusions

In summary, we developed a series of poly(terphenyl-*co*-dibenzothiophene ethylimidazole) (P(TP_x-DBT_{1-x}-EIm)) membranes via a one-step superacid-catalyzed polycondensation strategy. The incorporation of π-conjugated DBT units increased the free volume and introduced additional hydrogen-bonding sites through the lone pairs on sulfur atoms. This structural modification led to enhanced PA doping contents, improved microphase separation, and the formation of efficient proton transport channels, thereby boosting proton conductivity. The chemical structure of the copolymers was confirmed by ^{1}H NMR, FT-IR, and XPS spectroscopy. SEM imags revealed dense and homogeneous morphologies in both surface and cross-sectional sections, while AFM phase images further supported the development of well-defined microphase-separated domains. All membranes exhibited favorable oxidative and thermal stability. Among the tested samples, the P($TP_{0.9}$-$DBT_{0.1}$-EIm) membrane demonstrated an optimal combination of properties, including a high inherent viscosity (1.11 dL g^{-1}), robust mechanical strength (13.3 MPa), excellent acid doping content (215 %), and a high proton conductivity (0.109 S cm^{-1} at 180 °C). Notably, a single HT-

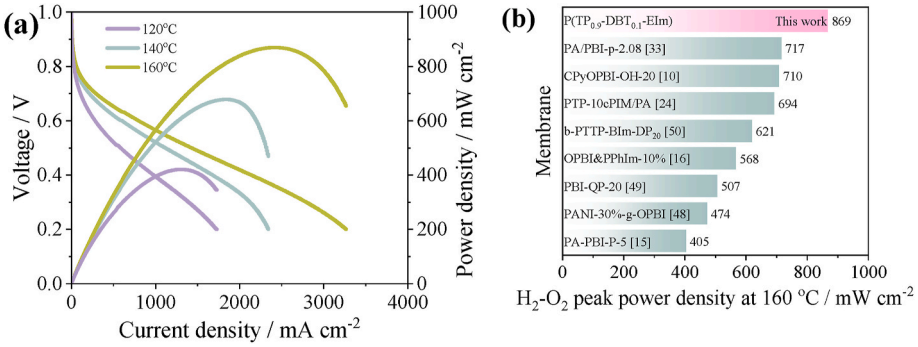

Fig. 7. (a) Polarization curve and power density based on the P($TP_{0.9}$-$DBT_{0.1}$-EIm)/215 % membrane at 120–160 °C under H_2–O_2 conditions without humidification and back pressure; (b) Comparison of H_2–O_2 peak power densities of different HT-PEMs at 160 °C.

PEMFC assembled with the P($TP_{0.9}$-$DBT_{0.1}$-EIm)/215 %PA membrane achieved a peak power density of 869 mW cm^{-2} at 160 °C under dry, non-pressurized H_2/O_2 conditions. In conclusion, the introduction of π-conjugated dibenzothiophene into the poly(arylene ethylimidazole) backbone effectively strengthened the hydrogen-bonding network, promoted favorable phase morphology, and facilitated proton transport, offering a promising strategy for advancing high-performance HT-PEMFC membranes.

CRediT authorship contribution statement

Jianan Su: Writing – original draft, Methodology, Investigation, Formal analysis, Data curation, Conceptualization. **Qi Liao:** Investigation, Data curation. **Lei Li:** Software, Methodology, Investigation. **Lili Sui:** Investigation, Data curation. **Jingshuai Yang:** Writing – review & editing, Writing – original draft, Supervision, Resources, Project administration, Funding acquisition, Conceptualization. **Jin Wang:** Writing – original draft, Methodology, Funding acquisition, Conceptualization.

Declaration of competing interest

The authors declare that they have no known competing financial interests or personal relationships that could have appeared to influence the work reported in this paper.

Acknowledgements

We gratefully acknowledge the Science and Technology Major Project of Liaoning Province (Grant No. 2024JH1/11700015) and Natural Science Foundation of China (52403273). We would like to express our gratitude to Prof. Yang Wu from Liaoning University for the assistance with the theoretical calculations.

Appendix A. Supplementary data

Supplementary data to this article can be found online at https://doi.org/10.1016/j.memsci.2025.124627.

Data availability

Data will be made available on request.

References

[1] Chinese society of electrochemistry, The top ten scientific questions in electrochemistry, J. Electrochem. 30 (2024) 2024121, https://doi.org/10.61558/2993-074X.3444.
[2] Y. Li, M. Chen, B. Lu, J. Zhang, Recent advances in exploring highly active & durable PGM-free oxygen reduction catalysts, J. Electrochem. 29 (2023) 2215002, https://doi.org/10.13208/j.electrochem.2215002.
[3] S. Wang, S. Jiang, Prospects of fuel cell technologies, Natl. Sci. Rev. 4 (2017) 163–166, https://doi.org/10.1093/nsr/nww099.
[4] Z. Chen, W. Zuo, K. Zhou, Q. Li, Y. Huang, J. E, Multi-factor impact mechanism on the performance of high temperature proton exchange membrane fuel cell, Energy 278 (2023) 127982, https://doi.org/10.1016/j.energy.2023.127982.
[5] Z. Guo, P. Maria, J. Chen, Z. ji, S.M. Holmes, Recent advances in phosphoric acid–based membranes for high–temperature proton exchange membrane fuel cells, J. Energy Chem. 63 (2021) 393–429, https://doi.org/10.1016/j.jechem.2021.06.024.
[6] P.C. Okonkwo, I.B. Belgacem, W. Emori, P.C. Uzoma, Nafion degradation mechanisms in proton exchange membrane fuel cell (PEMFC) system: a review, Int. J. Hydrogen Energy 46 (2021) 27956–27973, https://doi.org/10.1016/j.ijhydene.2021.06.032.
[7] D. Aili, D. Henkensmeier, S. Martin, B. Singh, Y. Hu, J.O. Jensen, L.N. Cleemann, Q. Li, Polybenzimidazole-based high-temperature polymer electrolyte membrane fuel cells: new insights and recent progress, Electrochem. Energy Rev. 3 (2020) 793–845, https://doi.org/10.1007/s41918-020-00080-5.
[8] Q. Li, J.O. Jensen, R.F. Savinell, N.J. Bjerrum, High temperature proton exchange membranes based on polybenzimidazoles for fuel cells, Prog. Polym. Sci. 34 (2009) 449–477, https://doi.org/10.1016/j.progpolymsci.2008.12.003.
[9] H. Sun, S. Wang, Y. Cui, Z. Yong, D. Liang, X. Wang, X. Wang, C. Li, F. Pan, Z. Wang, Branched polybenzimidazole/polymeric ionic liquid cross-linked membranes with high proton conductivity and mechanical properties for HT-PEM applications, Int. J. Hydrogen Energy 48 (2023) 5618–5629, https://doi.org/10.1016/j.ijhydene.2022.07.222.
[10] J. Ji, H. Li, W. Wang, J. Li, W. Zhang, K. Li, T. Yang, W. Jin, Y. Tang, W. Li, C. Gong, Silane-crosslinked polybenzimidazole with different hydroxyl content for high-temperature proton exchange membrane, J. Membr. Sci. 694 (2024) 122423, https://doi.org/10.1016/j.memsci.2024.122423.
[11] J. Dai, Y. Zhang, Y. Zhuang, G. Wang, Structural architectures of polymer proton exchange membranes suitable for high-temperature fuel cell applications, Sci. China Mater. 65 (2022) 273–297, https://doi.org/10.1007/s40843-021-1889-8.
[12] G. Liu, H. Pan, S. Zhao, Y. Wang, H. Tang, H. Zhang, Grafting of amine end-functionalized side-chain polybenzimidazole acid–base membrane with enhanced phosphoric acid retention ability for high-temperature proton exchange membrane fuel cells, Molecules 29 (2024) 340, https://doi.org/10.3390/molecules29020340.
[13] Y. Devrim, G.N.B. Durmuş, Composite membrane by incorporating sulfonated graphene oxide in polybenzimidazole for high temperature proton exchange membrane fuel cells, Int. J. Hydrogen Energy 47 (2022) 9004–9017, https://doi.org/10.1016/j.ijhydene.2021.12.257.
[14] H. Guo, Z. Li, H. Pei, P. Sun, L. Zhang, P. Li, X. Yin, Stable branched polybenzimidazole high temperature proton exchange membrane crosslinking and pentaphosphonic-acid doping lower fuel permeability and enhanced proton transport, J. Membr. Sci. 644 (2022) 120092, https://doi.org/10.1016/j.memsci.2021.120092.
[15] H. Sun, J. Bao, G. Pan, H. Cao, H. Wang, Z. Ji, Preparation and properties of polybenzimidazole proton exchange membranes with hydrogen bond-rich networks formed by branches, Int. J. Hydrogen Energy 81 (2024) 1192–1197, https://doi.org/10.1016/j.ijhydene.2024.05.390.
[16] X. Sun, H. Yu, J. Guan, B. Zhang, J. Zheng, S. Li, S. Zhang, The impact of imidazolium with steric hindrance on the dissociation of phosphoric acid and the performance of high-temperature proton exchange membranes, J. Mater. Chem. A 12 (2024) 24499–24507, https://doi.org/10.1039/D4TA03948C.
[17] G. Li, C. Zhao, C. Zhu, C. Ru, X. Li, D. Qi, Y. Wei, H. Na, Side-chain-type quaternized naphthalene-based poly (arylene ether ketone) s for anhydrous high temperature proton exchange membranes, RSC Adv. 6 (2016) 98854–98860, https://doi.org/10.1039/C6RA08072C.
[18] J. Yang, J. Wang, C. Liu, L. Gao, Y. Xu, Q. Che, R. He, Influences of the structure of imidazolium pendants on the properties of polysulfone-based high temperature proton conducting membranes, J. Membr. Sci. 493 (2015) 80–87, https://doi.org/10.1016/j.memsci.2015.06.010.
[19] R. Liu, M. Liu, S. Wu, X. Che, J. Dong, J. Yang, Assessing the influence of various imidazolium groups on the properties of poly(vinyl chloride) based high temperature proton exchange membranes, Eur. Polym. J. 137 (2020) 109948, https://doi.org/10.1016/j.eurpolymj.2020.109948.
[20] H. Tang, K. Geng, J. Hao, X. Zhang, Z. Shao, N. Li, Properties and stability of quaternary ammonium-biphosphate ion-pair poly(sulfone)s high temperature proton exchange membranes for H_2/O_2 fuel cells, J. Power Sources 475 (2020) 228521, https://doi.org/10.1016/j.jpowsour.2020.228521.
[21] Z. Lv, N. Zhao, M. He, Q. Ju, G. Chao, Y. Wang, K. Geng, H. Tang, N. Li, The effect of high-temperature proton exchange membranes with microphase separation structure on phosphoric acid loss, J. Membr. Sci. 687 (2023) 122075, https://doi.org/10.1016/j.memsci.2023.122075.
[22] L. Huang, Q. Wang, Z. Wang, X. Sun, J. Guan, J. Zheng, S. Li, S. Zhang, One-pot preparation of crosslinked network membranes via knitting strategy for application in high-temperature proton-exchange membrane fuel cells, J. Mater. Chem. A 12 (2024) 13364–13373, https://doi.org/10.1039/D4TA00243A.
[23] H. Bai, H. Peng, Y. Xiang, J. Zhang, H. Wang, S. Lu, L. Zhuang, Poly(arylene piperidine)s with phosphoric acid doping as high temperature polymer electrolyte membrane for durable, high-performance fuel cells, J. Power Sources 443 (2019) 227219, https://doi.org/10.1016/j.jpowsour.2019.227219.
[24] B. Liu, Y. Duan, T. Li, Y. Pang, Q. Liu, Q. Li, X. Hu, C. Zhao, Poly (triphenylene-piperidine) membranes reinforced by carboxy intrinsic microporous polymers towards high output power at low phosphoric acid levels for HT-PEMFC, J. Membr. Sci. 692 (2024) 122273, https://doi.org/10.1016/j.memsci.2023.122273.
[25] Y. Jin, T. Wang, X. Che, J. Dong, Q. Li, J. Yang, Poly (arylene pyridine) s: new alternative materials for high temperature polymer electrolyte fuel cells, J. Power Sources 526 (2022) 231131, https://doi.org/10.1016/j.jpowsour.2022.231131.
[26] R. Lv, S. Jin, L. Li, Q. Wang, L. Wang, J. Wang, J. Yang, The influence of comonomer structure on properties of poly(aromatic pyridine) copolymer membranes for HT-PEMFCs, J. Membr. Sci. 701 (2024) 122703, https://doi.org/10.1016/j.memsci.2024.122703.
[27] N. Shi, G. Wang, Q. Wang, L. Wang, Q. Li, J. Yang, Acid doped branched poly (biphenyl pyridine) membranes for high temperature proton exchange membrane fuel cells and vanadium redox flow batteries, Chem. Eng. J. 489 (2024) 151121, https://doi.org/10.1016/j.cej.2024.151121.
[28] Q. Wang, S. Zhao, Y. Guo, W. Wei, L. Wang, J. Yang, High-performance poly (aromatic pyridine) copolymers with crown ether moieties for high temperature polymer electrolyte membrane fuel cells, Sci. China Chem. 68 (2025) 1078–1090, https://doi.org/10.1007/s11426-024-2269-0.
[29] Q. Wang, Z. Zhang, P. Lv, Z. Peng, J. Yang, Poly(terphenyl pyridine) based amphoteric and anion exchange membranes with high ionic selectivity for vanadium redox flow batteries, Chem. Eng. J. 505 (2025) 158922, https://doi.org/10.1016/j.cej.2024.158922.
[30] D. Seo, Y.D. Lim, M.A. Hossain, S.H. Lee, H.C. Lee, H.H. Jang, M.M. Islam, W. G. Kim, Phosphoric acid doped sulfonated poly(tetra phenyl isoquinoline ether

sulfone) copolymers for high temperature proton exchange membrane potential application, Int. J. Hydrogen Energy 38 (2013) 667–674, https://doi.org/10.1016/j.ijhydene.2012.05.162.
[31] K.J. Kallitsis, R. Nannou, A.K. Andreopoulou, M.K. Daletoub, D. Papaioannoua, S. G. Neophytidesb, J.K. Kallitsis, Crosslinked wholly aromatic polyether membranes based on quinoline derivatives and their application in high temperature polymer electrolyte membrane fuel cells, J. Membr. Sci. 379 (2018) 144–154, https://doi.org/10.1016/j.jpowsour.2018.01.034.
[32] H. Cho, J. Seiler, P. Atanasova, V. Atanasov, Ion-pair membrane based on Imidazolium-functionalized poly (pentafluorostyrene) for high-temperature proton exchange membrane fuel cell application, ACS Appl. Energy Mater. 7 (2024) 1864–1872, https://doi.org/10.1021/acsaem.3c02854.
[33] J. Lin, P. Wang, A. Gao, J. Luo, Z. Li, L. Wang, X. Peng, An imidazole-philic dispersible ionic liquid provides ample proton transport channels and high proton performances for high temperature proton exchange membranes, Chem. Eng. J. 475 (2023) 146146, https://doi.org/10.1016/j.cej.2023.146146.
[34] T. Mu, L. Wang, Q. Wang, Y. Wu, P. Jannasch, J. Yang, High-performance imidazole-containing polymers for applications in high temperature polymer electrolyte membrane fuel cells, J. Energy Chem. 98 (2024) 512–523, https://doi.org/10.1016/j.jechem.2024.07.017.
[35] L. Wang, Q. Wang, P. Lv, Z. Peng, J. Yang, Synthesis of poly(terphenyl-co-dibenzo-18-crown-6 methylimidazole) copolymers for high-performance high temperature polymer electrolyte membrane fuel cells, J. Membr. Sci. 714 (2025) 123416, https://doi.org/10.1016/j.memsci.2024.123416.
[36] L. Wang, S. Celenk, Q. Wang, Q. Li, J. Yang, Long-durability poly(dibenzofuran-co-terphenyl N-methylimidazole) copolymer membranes for high-temperature polymer electrolyte membrane fuel cells, Macromolecules 58 (2025) 5344–5355, https://doi.org/10.1021/acs.macromol.5c00024.
[37] W. Zheng, L. He, T. Tang, R. Ren, H. Lee, G. Ding, L. Wang, L. Sun, Poly (dibenzothiophene-terphenyl piperidinium) for high-performance anion exchange membrane water electrolysis, Angew. Chem. Int. Ed. 63 (2024) e202405738, https://doi.org/10.1002/anie.202405738.
[38] J. Gao, J. Zhao, J. Wu, Y. Lei, N. Li, J. Yu, Z. Sui, Y. Wang, J. Yang, Z. Wang, Preparation of highly conductive anion exchange membranes by introducing dibenzothiophene monomer into the polymer backbone, J. Power Sources 602 (2024) 234314, https://doi.org/10.1016/j.jpowsour.2024.234314.
[39] Z. Peng, T. Wei, Q. Wang, Y. Zhao, J. Yang, Fabrication and investigation of anion exchange membranes based on poly(terphenyl piperidonium) copolymers with dibenzothiophene or dibenzofuran units for water electrolysis, J. Power Sources 642 (2025) 236918, https://doi.org/10.1016/j.jpowsour.2025.236918.
[40] J. Yang, L.N. Cleemann, T. Steenberg, C. Terkelsen, Q. Li, J.O. Jensen, H.A. Hjuler, N.J. Bjerrum, R. He, High molecular weight polybenzimidazole membranes for high temperature PEMFC, Fuel Cells 14 (1) (2014) 7–15, https://doi.org/10.1002/fuce.201300070.
[41] Z. Peng, B. Zhao, X. Cheng, M. Zhang, J. Yang, Poly(arylene piperidine) copolymer membranes with π-conjugated heterocycles for high temperature polymer electrolyte membrane fuel cells, Int. J. Hydrogen Energy 149 (2025) 150064, https://doi.org/10.1016/j.ijhydene.2025.150064.
[42] S. Jayalakshmi, S. Perumal, D.A. Wilson, Proton and carbon NMR spectra of 2-substituted dibenzothiophenes, Magn. Reson. Chem. 27 (1989) 684–686, https://doi.org/10.1002/mrc.1260270715o.
[43] S. Sarkar, P.K. Sruthi, N. Ramanathan, K. Sundararajan, Strong proton-shared hydrogen bonding in a methyl imidazole···HCl complex evidence from matrix isolation infrared spectroscopy and ab initio computations, New J. Chem. 44 (2020) 7116–7128, https://doi.org/10.1039/D0NJ00029A.
[44] Q. Wang, T. Wei, Z. Peng, Y. Zhao, P. Jannasch, J. Yang, High-performance anion exchange membranes based on poly(oxindole benzofuran dibenzo-18-crown-6)s functionalized with hydroxyl and quaternary ammonium groups for alkaline water electrolysis, J. Colloid Interface Sci. 686 (2025) 304–317, https://doi.org/10.1016/j.jcis.2025.01.244.
[45] T. Stamenković, N. Bundaleski, T. Barudžija, I. Validžić, V. Lojpur, XPS study of iodine and tin doped Sb_2S_3 nanostructures affected by non-uniform charging, Appl. Surf. Sci. 567 (2021) 150822, https://doi.org/10.1016/j.apsusc.2021.150822.
[46] G. Krishna V S, M.G. M, XPS analysis of $ZnS_{0.4}Se_{0.6}$ thin films deposited by spray pyrolysis technique, J. Electron. Spectrosc. Relat. Phenom. 249 (2021) 147072, https://doi.org/10.1016/j.elspec.2021.147072.
[47] N. Seselj, D. Aili, S. Celenk, L.N. Cleemann, H.A. Hjuler, J.O. Jensen, K. Azizi, Q. Li, Performance degradation and mitigation of high temperature polybenzimidazole based polymer electrolyte membrane fuel cells, Chem. Soc. Rev. 52 (2023) 4046–4070, https://doi.org/10.1039/D3CS00072A.
[48] Y. Xiao, Q. Ma, X. Shen, S. Wang, J. Xiang, L. Zhang, P. Cheng, X. Du, Z. Yin, N. Tang, Facile preparation of polybenzimidazole membrane crosslinked with three-dimensional polyaniline for high-temperature proton exchange membrane, J. Power Sources 528 (2022) 231218, https://doi.org/10.1016/j.jpowsour.2022.231218.
[49] Y. You, X. Deng, Q. Liu, Y. Hou, S. Miao, A semi-flexible polybenzimidazole with enhanced comprehensive performance for high-temperature proton exchange membrane fuel cells, Int. J. Hydrogen Energy 78 (2024) 879–888, https://doi.org/10.1016/j.ijhydene.2024.06.324.
[50] Y. Li, Z. Xu, W. Shi, M. Wang, Z. Lin, D. He, Y. Pan, J. Liao, E.H. Ang, J. Shen, Branched poly(terphenyl trifluoroacetophenone piperidone) membranes with dual-proton conductor assist for enhancing fuel cell performance operation in high-temperature, J. Membr. Sci. 727 (2025) 124127, https://doi.org/10.1016/j.memsci.2025.124127.
[51] J. Chen, W. Du, Z. Guo, X. Lu, M.P. Tudball, X. Yang, Z. Zhou, S. Zhou, A. Rack, B. Lukic, P.R. Shearing, S.J. Haigh, S.M. Holmes, T.S. Miller, Decoupling membrane electrode assembly materials complexity from fuel cell performance through image-based multiphase and multiphysics modelling, Adv. Energy Mater. 15 (2025) 2405179, https://doi.org/10.1002/aenm.202405179.
[52] J. Chen, X. Lu, L. Wang, W. Du, H. Guo, M. Rimmer, H. Zhai, Y. Liu, P.R. Shearing, S.J. Haigh, S.M. Holmes, T.S. Miller, Laser scribed proton exchange membranes for enhanced fuel cell performance and stability, Nat. Commun. 15 (2024) 10811, https://doi.org/10.1038/s41467-024-55070-8.
[53] J. Chen, M. Perez-Page, C.M.A. Parlett, Z. Guo, X. Yang, Z. Zhou, H. Zhai, S. Bartlett, T.S. Miller, S.M. Holmes, Operando synchrotron-based X-ray study and intervention approaches of graphene-related-materials for investigating the performance and durability of HT-PEMFC, Chem. Eng. J. 487 (2024) 150670, https://doi.org/10.1016/j.cej.2024.150670.